

Towards Lossless Ultimate Vision Token Compression for VLMs

Dehua Zheng, Mouxiao Huang, Borui Jiang, Hailin Hu, Xinghao Chen
Huawei Noah’s Ark Lab

{zhengdehua2, huangmouxiao, jiangborui, hailin.hu, xinghao.chen}@huawei.com

Abstract

Visual language models encounter challenges in computational efficiency and latency, primarily due to the substantial redundancy in the token representations of high-resolution images and videos. Current attention/similarity-based compression algorithms suffer from either position bias or class imbalance, leading to significant accuracy degradation. They also fail to generalize to shallow LLM layers, which exhibit weaker cross-modal interactions. To address this, we extend token compression to the visual encoder through an effective iterative merging scheme that is orthogonal in spatial axes to accelerate the computation across the entire VLM. Furthermore, we integrate a spectrum pruning unit into LLM through an attention/similarity-free low-pass filter, which gradually prunes redundant visual tokens and is fully compatible to modern FlashAttention. On this basis, we propose *Lossless Ultimate Vision tokens Compression (LUVC)* framework. LUVC systematically compresses visual tokens until complete elimination at the final layer of LLM, so that the high-dimensional visual features are gradually fused into the multimodal queries. The experiments show that LUVC achieves a $2\times$ speedup inference in language model with negligible accuracy degradation, and the training-free characteristic enables immediate deployment across multiple VLMs.

1. Introduction

In recent years, the extensive deployment of large language models (LLM) in visual domains has catalyzed significant progress in visual language models (VLM) [2, 6, 18, 32]. VLM typically adopts a framework comprising visual encoder [33, 52] and projector to achieve cross-modal alignment between textual and visual domains. Consequently, VLMs have demonstrated robust performance across diverse downstream applications, encompassing visual question answering, spatial localization, and temporal reasoning tasks. However, VLMs suffer from prohibitive inference costs due to their massive parameterization (often in the billions) and quadratic computational complexity with

respect to input sequence length. The sequence length of high-resolution images and videos further exacerbates this issue [5], and becomes the primary bottleneck. These constraints severely limit the real-time deployment of VLMs in practical applications.

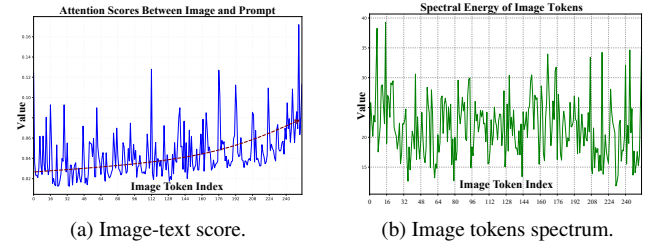


Figure 1. The distribution of image-text attention scores and tokens spectrum. Due to position bias, the attention scores exhibit a significant upward trend near the text region, whereas the spectrum curve remains position-invariant.

Extensive research has been devoted to compressing visual tokens to mitigate redundancy and accelerate the inference process of LLM. These approaches fundamentally operate either at projector or within the LLM, eliminating or merging redundant visual tokens based on similarity metrics or attention score ranking mechanisms. We systematically examine these approaches through two methodological foundations while critically evaluating their inherent limitations. (1) Attention-aware pruning. These approaches primarily employ either special token (eg. [CLS]) or text-guided attention to rank the importance of visual tokens. For example, FastV [5] and SparseVLM [56] develop text-guided compression algorithms based on cross-modal attention between visual and textual tokens. However, these methods suffer from significant position bias [43, 55]. As illustrated in Fig. 1a, position bias introduces substantial noise in importance estimation, tokens adjacent to text consistently exhibit inflated attention weights regardless of their semantic relevance. Furthermore, due to reliance on explicit attention score, these compression methods cannot be accelerated using modern FlashAttention [8] optimization techniques. (2) Similarity-aware merging. These methods typically compute the similarity between tokens

and employ bipartite matching [3, 47, 53] or clustering-based [9, 13] approaches for vision token compression. However, their computational efficiency significantly deteriorates when processing longer vision token sequences. Additionally, these compression algorithms focus solely on local token-wise proximity while neglecting the global information distribution. They tend to excessively merge tokens in dense regions while inadequately merging them in sparse regions, thereby compromising semantic integrity and class balance, leading to distributional shift [15]. Moreover, clustering-based approaches disrupt the original positional arrangement of tokens, resulting in disordered spatial information.

Additionally, early-layer LLM pruning risks semantic degradation, forcing most methods to only prune deeper LLM layers while keeping visual encoder, projectors and early LLMs intact. Despite attempts [27] to integrate a limited number of visual tokens in the visual encoder, existing methods compromise spatial structure and remain incompatible with versatile 2D projector architectures. Thus, token compression across the entire VLM remains largely unexplored.

To overcome the above limitations, we propose a more robust and resilient algorithm towards **Lossless Ultimate Vision token Compression (LUVVC)**, which operates across the entire network and is training-free. LUVVC extends token compression to the visual encoder through a computationally efficient **Orthogonal Iterative Merger (OIM)** and eliminates noisy tokens through a **Spectrum Pruning Unit (SPU)** equipped with a carefully crafted low-pass filter in LLM. As shown in Fig. 1b, visual token spectrum exhibits robustness against position bias, which provides reliable grounding for stable pruning unlike attention weights. Existing researchs [37, 40] have empirically verified the inherent high-frequency attenuation property in Transformer architectures during forward propagation, providing additional theoretical support for our frequency-based SPU. As shown in Fig. 2, visualization reveals that low-frequency features exhibit a concentrated distribution in visually salient regions, which further corroborates the feasibility of frequency-based pruning. For the compression during visual encoder, OIM performs iterative merging that is orthogonal in spatial. OIM maintains the intrinsic spatial structure of visual inputs, ensuring compatibility with various projector architectures, while simultaneously increasing parallelizability for more computationally efficient processing. Our contributions are as follows:

- Based on the spectrum characteristics of Transformer features, we design the attention/similarity-free spectrum pruning unit (SPU), which gradually prune high-frequency noise tokens until all visual information is fused into the multimodal queries, achieving ultimate pruning of visual tokens at the final LLM layer.



Figure 2. Visualization of low-frequency visual tokens of Internvl2.5-8B in layer-8.

- We design the orthogonal iterative merger (OIM) that merges tokens in spatial axes to reduce the computation across the entire VLM. OIM maintains the spatial structure of visual input and is suitable for diverse projectors.
- We integrate the above two strategies to construct training-free LUVVC, achieving approximately 2× acceleration while maintaining nearly lossless performance. Experimental results confirm that the plug-and-play LUVVC demonstrates remarkable compatibility across diverse VLM architectures and parameter scales, while achieving superior performance on diverse tasks including single image, multi images, videos, and particularly information-dense chart and document processing.

2. Related Work

2.1. Multimodal Large Language Models

VLM architectures have diversified in design. Taking projectors as an example, the BLIP [19, 20] and MiniCPM-V2.6 [48] employ cross-attention mechanisms. The LLaVA series [18, 25] introduce a two-layer MLP to bridge visual and language models. InternVL2.5 [6] and Qwen2.5-VL [2] employ pixel shuffle and token merger modules, respectively, which necessitates preservation of spatial structural information. The evolutionary trajectory of these models has progressed from rudimentary image comprehension to encompass a broad spectrum of downstream applications. This expansion has engendered specialized model variants, including video-oriented architectures [16, 23, 42] and document analysis systems [12, 54], each tailored to their respective domains. Gemin [1] and LWM [26] have established long-context modeling as a fundamental capability. This theoretical advancement has catalyzed significant progress in high-resolution image and long-form video understanding. This paradigm presents critical challenges for model efficiency, mandating the development of sophisticated token compression methodologies.

2.2. Vision Token Compression Methods

Numerous token pruning techniques, inspired by traditional visual transformers pruning [34, 46, 57], or novel token compression schemes for VLMs, have been proposed to accelerate inference. FastV [5] was the first to explore redun-

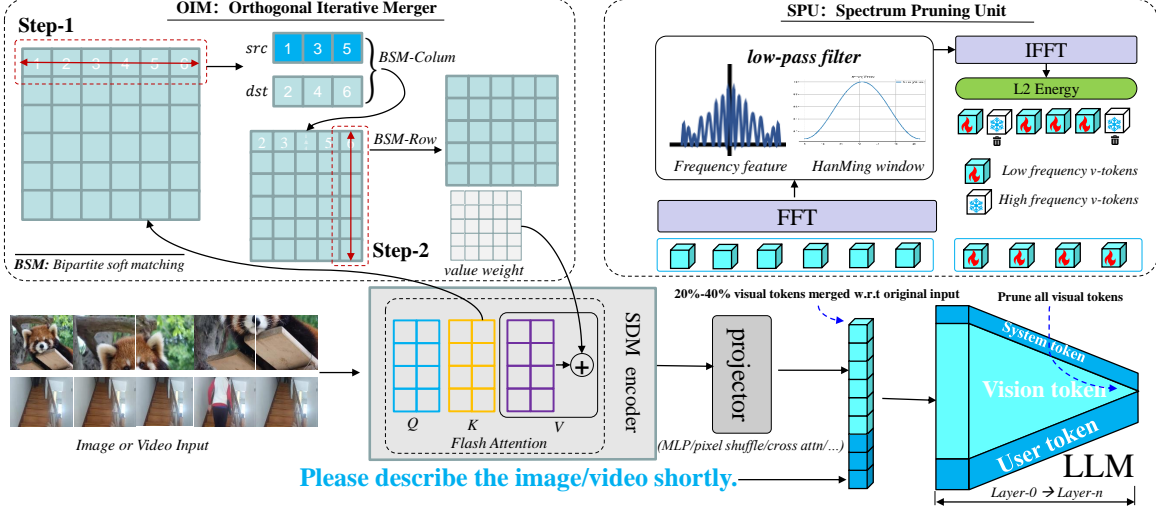


Figure 3. The overview of LUVV. LUVV consists of two key components. (1) Orthogonal Iterative Merger (OIM), which maintains the spatial structure while increasing computational parallelism by performing step-by-step merging in both lateral and longitudinal dimensions. (2) Spectrum Pruning Unit (SPU), which applies low-pass filtering to visual tokens through FFT and IFFT, which achieves progressive token pruning via cascade structure.

dant visual tokens using text-guided attention score. FasterVLM [55] introduced an alternative approach by utilizing the attention of the [CLS] token. SparseVLM [56] further improved upon FastV by performing an initial screening of visual queries and recovering pruned visual tokens. Some works have adopted various advanced techniques during the training phase. For instance, Qwen2-VL [41] adopts a token merging strategy during training, where four spatially adjacent patches are aggregated into a single consolidated visual token. MiniCPM-V2.6 [48] introduces trainable queries, which dynamically projects visual segments into fixed-dimensional latent representations. While these approaches require sophisticated end-to-end training frameworks with non-trivial computational overhead, and limit applicability exclusively to proprietary model, precluding generalization to open-source or third-party VLMs. FastVLM [38] innovatively integrates FastViTHD to maintain high-resolution image processing capabilities while producing fewer output tokens. VTW [24] demonstrated that visual tokens can be aggressively pruned at the final stage of LLMs, a finding validated on several simple vision benchmarks. Additionally, various clustering-based methods merge similar tokens based on semantic similarity and static distance, such as Chat-UniVi [13], PACT [9], and LLaVA-PruMerge [35]. However, due to inherent limitations, these algorithms cannot achieve optimal performance. To overcome these limitations, we designed an innovative pruning framework LUVV through a spectrum pruner and an orthogonal iterative merge.

3. Methodology

In this section, we provide a detailed introduction to the LUVV method, as illustrated in the Fig. 3. This method achieves the complete elimination of visual tokens by merging similar tokens during the visual encoder and gradually filtering out high-frequency tokens during the LLM, ultimately integrating all low-frequency, high-information visual tokens into the multimodal query. The LUVV consists of two core components. First, an orthogonal iterative merger is designed during the visual encoder, performing iterative merging in spatial axes. Then, in the LLM phase, the merged visual tokens undergo spectrum analysis through Fast Fourier Transforms (FFT) and Inverse Fast Fourier transforms (IFFT), with a carefully designed low-pass filter progressively filtering out high-frequency noise tokens. Notably, spectrum pruning begins at an earlier layer of the LLM and is cascaded to cover the final layer. Section 3.1 3.1 provides a priori analysis, discussing the computational complexity of VLMs, and the importance of low-frequency visual tokens. Section 3.2 3.2 analyzes the design of the orthogonal iterative merger, while Section 3.3 3.3 details the design of the spectrum pruning unit and low-pass filter.

3.1. Preliminary Analyze

Computational Complexity Analysis. The *Flops* of VLMs primarily arise from the self-attention (SA) and feed-forward network (FFN). We define the $Flops = O(n^2d + nd^2)$, where $n = v_t + n_v$ is the total token sequence length

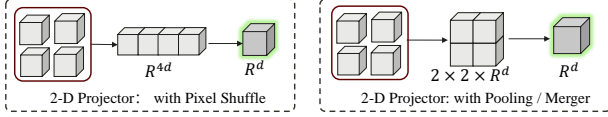


Figure 4. The examples of 2D projectors demonstrate that they rely on the 2D spatial structure.

and d is the hidden dimension. For InternVL-2.5, a frame or image patch generates $n_v = 256$ visual tokens. For a video with 32 frames, $n_v \approx 8 \times 10^3$, which is approximately two orders of magnitude greater than n_t . This excessive redundancy of n_v imposes substantial computational overhead during visual encoder and LLM. Meanwhile, we analyze the $Flops' = O(n_v^2 k)$ of traditional merge strategies, where k is the dimension of keys. In contrast, our OIM perform orthogonal merging in spatial axes. The visual tokens is transferred from $R^{1 \times n_v \times k}$ to $R^{\sqrt{n_v} \times \sqrt{n_v} \times k}$, $Flops' = O(n_v^{1.5} k)$, which is computationally more efficient and maintains the spatial structure.

The Importance of Low-frequency Visual Tokens.

Due to the global attention mechanism of Transformers, low-frequency visual tokens more extensive global and cross-modal information, which is more crucial for high-level semantics. In addition, low-frequency visual tokens are more robust to noise and minor disturbances, which avoids pruning errors caused by noise (such as translation, lighting changes). Numerous works [40, 49] have rigorously derived the mathematical characterization of this preference for low-frequency signals in Transformer. We define visual token $z \in \mathbf{R}^D$ and fourier feature $\sum_{n=0}^{N-1} z e^{-i2\pi kn/N}$, $DC[z](k=0)$ is Direct-current Component (DC) and $H[z](k=1, 2, \dots, N-1)$ is High-frequency Component (HC), A is the attention-weights. Formula 1 is a straightforward result of Perron-Frobenius theorem, which demonstrates that Transformer exhibit an inherent bias toward low-frequency components and treat high-frequency signals as noise or redundancy to gradually smooth them out.

$$\lim_{t \rightarrow \infty} \frac{\|HC[A^t z]\|_2}{\|DC[A^t z]\|_2} = 0 \quad [40] \quad (1)$$

In summary, low-frequency visual tokens contain more critical semantics and are less susceptible to noise interference, a theory further substantiated by Fig. 2.

3.2. Orthogonal Iterative Merger

Merging in one-dimensional space disrupts the spatial structure of the original visual input. As shown in the Fig. 4, many contemporary projector architectures operate natively in 2D spatial structure [2, 6], fundamentally precluding the application of traditional merging during the visual encoder due to dimensional incompatibility and spatial structure disruption. While dimensionality reduction can partially miti-

gate computational costs, significant resource overhead and latency persists, as discussed in Section 3.1 3.1. To address this, we design OIM to perform an effective iterative merging that is orthogonal in spatial axes, as illustrated in Fig. 3.

We define visual token sequence $X_v \in \mathbf{R}^{L \times D}$, where $L = H * W$, L is the sequence length, and H and W are the horizontal width and vertical height, respectively. Unlike ToMe which performs similarity computations in one-dimensional space, OIM iteratively merges tokens in spatial axes for more efficient processing. Initially, we conduct a row merge operation, altering the arrangement of the original tokens to obtain $X'_v \in \mathbf{R}^{H \times W \times D}$. After similarity calculations and binary matching, we acquire $X_v^1 \in \mathbf{R}^{H \times (W-m) \times D}$, m is the number of tokens merged per operation. Subsequently, we proceed with the column merge operation, similarly perform parallel calculations in the row dimension to obtain $X_v^2 \in \mathbf{R}^{(H-m) \times (W-m) \times D}$. Consequently, OIM achieves true 2D token merging that preserves the structural integrity of visual feature spaces while significantly improving computational parallelism, resulting in hardware-efficient processing.

Additionally, to explicitly differentiate the information density of various tokens and allocate varying levels of attention accordingly, we have adopted a value enhancement strategy. This approach mitigates reliance on attention weights, adapts to FlashAttention, and significantly enhances the handling of token quantities, which is formulated as Formula 3:

$$A = \text{softmax}\left(\frac{QK^T}{\sqrt{d}}\right) \quad (2)$$

$$O = A(V + \log(s)) \quad (3)$$

where s is a row vector containing the number of the merged token.

3.3. Spectrum Pruning Unit

The attention-based pruning strategy is incompatible with FlashAttention and exhibits substantial approximation errors [43], as positional biases systematically distort the evaluation of intrinsic information content of individual tokens. Furthermore, similarity-based methods that focus solely on token-wise proximity often disrupt class balance and the original arrangement of visual tokens. As theoretically analyzed in Section 3.1 3.1, low-frequency visual tokens capture more extensive global and cross-modal information, which is preferentially processed by the Transformer architecture. Additionally, frequency-domain transformation exhibits lower complexity and remains compatible with FlashAttention. Based on this, we design the spectrum pruning unit to progressively prune high-frequency noise tokens during the LLM. We define visual token $X_b[n] \in \mathbf{R}^D$, n represents the index of the visual token. We map $X_b[n]$ to

the frequency domain through FFT to analyze their spectrum characteristics through Formula 4.

$$X_b[k] = \sum_{n=0}^{N-1} X_b[n] e^{-i2\pi kn/N} \quad (4)$$

When applying FFT to visual tokens, we employ Hamming Window (Formula 5) to mitigate frequency leakage artifacts (e.g., spurious high-frequency components induced by row-column transformations). This spectrum smoothing technique progressively attenuates frequency features, suppressing abrupt transitions to yield more accurate spectrum representations that better approximate the true frequency distribution. We obtain a low-pass filter $M_b[k]$ through Formula 6 to remove high-frequency noise tokens.

$$M_b[k] = \begin{cases} 0.54 - 0.46 \cos(\frac{2\pi n}{N-1}), & k \leq \sigma_t \\ 0, & k > \sigma_t \end{cases} \quad (5)$$

$$X'_b[k] = X_b[k] M_b[k] \quad (6)$$

After smoothing with the Hamming Window and processing through a low-pass filter, LUVC obtained a more informative low-frequency visual component $X'_b[k]$. Subsequently, we transform $X'_b[k]$ into the original domain to obtain $X'_b[n]$ through the IFFT (Formula 7). Furthermore, we conduct an energy analysis on $X'_b[k]$ by Formula 8, specifically calculating the L2 norm of $X'_b[k]$, which effectively removes high-frequency noise tokens and returns low-frequency visual tokens with high information content.

$$X'_b[n] = \frac{1}{N} \sum_{k=0}^{N-1} X'_b[k] e^{i2\pi kn/N} \quad (7)$$

$$E_b[n] = \|X'_b[n]\|_2 \quad (8)$$

By employing this spectrum analysis method for pruning, we effectively eliminate redundant noise tokens and preserve important region, as illustrated in Fig. 2, thereby reducing memory usage and computational cost. Simultaneously, this approach provides more focused visual information for cross-modal interactions and aligns well with FlashAttention. Leveraging the feasibility of pruning all visual tokens in the final stages of LLMs as demonstrated by VTW [24], we integrate the spectrum pruning strategy into the cascade structure. This enables progressive attenuation of visual tokens in the LLM’s final stages, accomplishing complete elimination through a controlled, gradual process.

4. Experiments

4.1. Evaluation Datasets

We evaluate LUVC across diverse benchmarks encompassing video, single-image, and multi-image. Specifically, we

conduct performance comparisons on challenging pruning-resistant domains including document and chart comprehension. **Video Understanding.** For Video tasks, we evaluate VideoMME [10], MVBench [21], NextQA [45], SeedBench [17], MLVU [58] and LongVideoBench [44], where VideoMME, MLVU and LongVideoBench are long video benchmarks. **Single-Image Understanding.** We evaluate LUVC’s comprehensive multimodal capabilities across a range of image understanding benchmarks, including MMB (ZH/EN) [28], POPE [22], MMMU [51], MM-Start [4] and AI2D [14]. **Multi-Image Understanding.** We evaluate LUVC in multi-image perception and understanding across various multi-image benchmarks, including MuirBench [39], BLINK [11] and RealWorldQA [7]. **Chart and Document Understanding.** Due to compact spatial layouts and dense textual information, chart and document understanding pose challenging tasks for token compression, we evaluate ChartQA [29], DocVQA [30], InfoVQA [31] and TextVQA [36]. **Image Caption.** The caption task requires the preservation of more semantic information and exhibits lower tolerance for errors in token compression algorithms. We evaluate the caption capability of LUVC on the Flickr30K [50].

4.2. Evaluation Setup

To comprehensively validate the applicability of LUVC across different VLM architectures and parameter scales, we conducted evaluations on all benchmarks using four distinct models: LLaVA-OV-0.5B, LLaVA-OV-7B, InternVL-2.5-8B, and InternVL-2.5-26B. To rigorously demonstrate the algorithmic advantages of LUVC, we selected three representative baselines for comparison: FastV (a classical attention-score-based method), PACT (the state-of-the-art similarity clustering algorithm), and VTW (an ultimate pruning-based approach). For fair comparison, we carefully tuned the parameters of each algorithm to achieve optimal performance on VLMs while maintaining comparable acceleration ratios. In addition to standard benchmark metrics, we measured the prefill-phase latency and average pruning rate ($Red.Ratio = \frac{L_p}{L_o}$) for each algorithm, where L_p is the average visual token sequences after compression and L_o is the average visual token sequences without compression. Notably, we adhered to the original hyperparameter configurations in paper for LLaVA-OV-7B and InternVL2.5-8B, while performing additional tuning (as no official settings were provided) to optimize performance on LLaVA-OV-0.5B and InternVL2.5-26B.

For LUVC, regarding the video benchmark, we merge approximately 35%-40% of the tokens during the visual encoder. For single-image or multi-image benchmarks, we merge around 15%-20% of the tokens during the visual encoder. For chart and document comprehension benchmarks, to maintain sufficient information and spatial layout, we do

Table 1. Comparative of LUVc with FastV, VTW, and PACT. **Red. Ratio** denotes the average pruning ratio, **Latency** represents the prefill latency of the LLM, and **Speedup** indicates the acceleration ratio. Herein, * signifies that there is a significant discrepancy between the accuracy of the baseline model we reproduce. The best performance is highlighted in **bold**.

Method	Red. Ratio	Latency	Speedup	VideoMME	MVBench	NextQA	SeedBench	MLVU	LongVideo	Avg.
LlavaOV-0.5B	0.00%	0.0772	–	44	45.5	57.2	44.2	50.3	45.80	47.83
LlavaOV-0.5B*	0.00%	0.0772	–	43.74	47.1	57.13	44.16	44.13	47.42	47.28
+ FastV	41.67%	0.0711	1.00×	43.07	46.1	56.32	43.55	43.72	45.32	46.35
+ VTW	54.17%	0.0596	1.30×	41.37	44.88	53.84	43.86	41.24	44.35	44.92
+ PACT	48.05%	0.0642	1.20×	42.7	45.17	55.16	44.8	41.76	45.92	45.92
+ LUVc (ours)	58.46%	0.0610	1.27×	44.37	46.85	57.33	44.96	44.88	46.90	47.55
LlavaOV-7B	0.00%	0.5194	–	58.2	56.7	79.4	56.9	64.7	56.4	62.05
+FastV	42.86%	0.2693	1.93×	57.56	57.38	78.08	56.72	60.87	53.4	60.67
+VTW	57.14%	0.2524	2.06×	46.81	45	65.43	48.44	50.36	46.97	50.50
+PACT	55.88%	0.2711	1.92×	57.6	56.98	78.74	56.8	64.7	55.8	61.77
+ LUVc (ours)	62.32%	0.2583	2.01×	58.78	57.88	78.47	57.36	63.77	56.92	62.20
InternVL-2.5-8B	0.00%	1.2480	–	64.20	72	–	–	68.90	60.00	–
InternVL-2.5-8B*	0.00%	1.2480	–	64.50	73.25	83.43	66.41	71.80	62.30	70.28
+ VTW	56.25%	0.6482	1.93×	62.81	70.8	80.99	65.45	69.32	60.36	68.29
+ PACT	55.41%	0.6949	1.80×	63.48	71.35	82.3	65.18	70.15	60.43	68.82
+ LUVc (ours)	62.12%	0.6293	1.98×	64.56	71.73	82.74	65.85	72.49	62.45	69.97
InternVL-2.5-26B	0.00%	2.9142	–	66.9	75.2	–	–	72.3	59.9	–
InternVL-2.5-26B*	0.00%	2.9142	–	66.9	76.47	86.24	71.41	75.11	62.75	73.15
+ VTW	66.67%	1.2586	2.32×	64.56	72.43	84.46	70.96	73	61.18	71.10
+PACT	59.61%	1.3548	2.15×	65.25	75.3	85.52	70.24	73.96	60.43	71.78
+ LUVc (ours)	61.32%	1.2255	2.38×	66.63	76.13	85.63	71.28	75.23	61.93	72.81

Table 2. Result of LUVc and other compress strategies for image benchmarks. The best performance is highlighted in **bold**.

Method	Red. Ratio	Latency	Speedup	Single Image						Multi Image			Avg.
				MMB(EN)	MMB(ZH)	POPE	MMStar	MMUVal	AI2D	MuirBench	BLINK	RealWorld	
LlavaOV-0.5B	0.00%	0.0462	–	52.1	–	–	37.5	31.4	57.1	25.5	–	55.6	–
LlavaOV-0.5B*	0.00%	0.0462	–	51.89	45.7	88.32	38.4	32.33	57.1	25.5	–	55.42	49.33
+FastV	41.67%	0.0498	0.93×	51.55	43.21	87.09	39.41	32.33	56.64	26.69	–	54.51	48.93
+VTW	54.17%	0.0398	1.16×	49.4	45.1	72.56	38.11	31.56	55.18	25.58	–	47.71	45.65
+PACT	48.05%	0.0503	0.92×	50.6	43.04	86.06	39.06	32.78	55.34	25.62	–	53.73	48.28
+LUVc (ours)	49.55%	0.0470	0.98×	51.72	44.59	88.04	39.13	32.56	56.22	24.88	–	56.47	49.20
LlavaOV-7B	0.00%	0.1927	–	80.8	80.4	89.17	61.7	48.8	81.4	41.8	–	66.3	68.90
+FastV	42.86%	0.1196	1.61×	79.21	79.64	88.83	58.56	48.67	79.53	41.12	–	64.18	67.47
+VTW	57.14%	0.1023	1.88×	58.59	57.99	50.97	39.34	43.78	69.43	34.85	–	41.7	49.58
+PACT	55.88%	0.1096	1.76×	80.3	79.98	88.93	59.79	48	80.86	43.1	–	64.71	68.21
+LUVc (ours)	53.97%	0.1205	1.60×	80.58	80.58	89.39	62.24	47.89	81.54	42.46	–	65.62	68.79
InternVL-2.5-8B	0.00%	0.2985	–	84.6	82.6	90.6	62.8	56	84.5	–	54.8	70.1	73.25
InternVL-2.5-8B*	0.00%	0.2985	–	83.85	83.59	88.91	62.93	53.44	84.68	–	54.6	70.45	72.81
+ VTW	56.25%	0.1369	2.18×	83.08	81.44	86.09	57.33	52	82.84	–	52.44	63.66	69.86
+PACT	55.41%	0.1721	1.73×	83.5	82.39	88.21	61.06	53.11	83.48	–	52.5	67.45	71.46
+LUVc (ours)	56.89%	0.1479	2.02×	83.85	83.25	89.19	61.4	53.22	84.1	–	54.87	69.41	72.41
InternVL-2.5-26B	0.00%	0.7072	–	85.4	85.5	90.6	66.5	60	86.4	–	61.8	74.5	76.34
InternVL-2.5-26B*	0.00%	0.7072	–	86.08	85.14	90.3	66.53	53.44	86.46	–	61.91	75.95	75.73
+VTW	66.67%	0.3150	2.25×	84.88	83.76	90.09	59.73	52.67	84.88	–	59.02	70.07	73.14
+PACT	59.61%	0.3544	2.00×	84.7	84.45	90.12	62.46	53.11	85.36	–	59.23	72.03	73.93
+LUVc (ours)	55.1%	0.3379	2.09×	84.97	84.45	90.32	65.2	53	85.72	–	61.75	74.9	75.04

not perform OIM. **Additional experimental details and results on QwenVL2.5 will be provided in the supplementary material.**

4.3. Main Results

Video Understanding. We conducted a comparative evaluation of LUVc, FastV, VTW, and PACT based on the LLaVA-OV series. Notably, since FlashAttention was enabled during the testing of InternVL2.5, we do not compare FastV on InternVL2.5. As shown in Table 9, LUVc demonstrates superior video understanding performance compared to other pruning algorithms while maintaining a similar speedup. Specifically, LUVc achieves lossless performance

across all LLaVA-OV series models. For the InternVL2.5 series, it incurs only a marginal accuracy degradation of approximately 0.3%, substantially outperforming the sub-optimal PACT algorithm. Taking InternVL2.5-8B as an example, LUVc exhibits average video understanding metrics that surpass VTW and PACT by 1.68% and 1.15%, respectively.

Single-Image Understanding and Multi-Images Understanding. For both single-image and multi-image benchmarks, LUVc maintains its performance advantage, achieving state-of-the-art results across evaluations on the LLaVA-OV and InternVL2.5, as shown in Table 2. Taking InternVL2.5-8B as an example, LUVc surpasses VTW and

Table 3. Comparison between LUVC and other token compression methods in chart and document tasks.

Method	Latency	Speedup	ChartQA	DocVQA	InfoVQA	TextVQA	Avg.
InternVL-2.5-8B	0.2985	—	84.8	—	—	79.1	—
InternVL-2.5-8B*	0.2985	—	83.36	91.96	75.45	78.99	82.44
+ VTW	0.1804	1.65	76.08	80.59	67.94	60.83	71.36
+ PACT	0.1980	1.51	75.96	84.32	64.67	72.73	74.72
+ LUVC (ours)	0.1857	1.61	82.44	91.48	74.75	77.80	81.62
InternVL-2.5-26B	0.7454	—	87.2	—	—	82.4	—
InternVL-2.5-26B*	0.7454	—	85.4	93.78	78.98	83.26	85.36
+ VTW	0.4637	1.61	82.24	88.78	75.52	73.33	79.97
+ PACT	0.4690	1.59	76.36	85.79	68.46	78.56	77.29
+ LUVC (ours)	0.4302	1.73	85.16	92.70	77.55	80.03	83.86

Table 4. Comparison between LUVC and other token compression methods in caption tasks Flickr30K [50].

Method	Speedup	BLEU-1	BLEU-2	METEOR	ROUGE-L	CIDEr	SPICE
InternVL-2.5-8B	—	0.248	0.156	0.139	0.329	0.669	0.236
+ VTW	1.65	0.203	0.119	0.115	0.291	0.448	0.191
+ PACT	1.51	0.231	0.144	0.133	0.32	0.602	0.23
+ LUVC (ours)	1.61	0.243	0.154	0.137	0.33	0.666	0.235
InternVL-2.5-26B	—	0.255	0.159	0.140	0.328	0.666	0.234
+ VTW	1.61	0.242	0.149	0.132	0.321	0.601	0.224
+ PACT	1.59	0.24	0.149	0.134	0.32	0.63	0.229
+ LUVC (ours)	1.73	0.25	0.156	0.138	0.326	0.664	0.232

PACT by 2.55% and 0.95%, respectively, in average video metrics. Notably, in the multi-image evaluation of the InternVL2.5 series, LUVC significantly outperforms the sub-optimal PACT algorithm by over 2%. These results further validate the generalizability of the LUVC algorithm across different evaluation tasks and model architectures.

4.4. Extra Experiments for Chart and Document Tasks

Chart and document comprehension tasks impose stringent demands on localized details and spatial layouts in images, presenting challenges for compression algorithms. To assess the efficacy of LUVC, we conduct benchmark evaluations using the InternVL2.5 model series on four challenging datasets: ChartQA, DocVQA, InfoVQA, and TextVQA. Due to task complexity, we sacrifice partial acceleration benefits during evaluation. Specifically, we disable the OIM in LUVC and substantially delay the pruning layers in both PACT and VTW to prevent performance collapse. As illustrated in Table 3, under similar latency, PACT and VTW still exhibit unacceptable performance degradation, whereas LUVC maintains a stronger performance advantage.

4.5. Extra Experiments for Image Captioning Task

The captioning capability provides a critical measure of whether key visual semantics are effectively preserved. To further demonstrate the generalization ability of LUVC, we conducted additional experiments on the Flickr [50] captioning task. The experimental results are summarized in

the Table 4, where a comparative analysis was performed based on InternVL2.5—8B/26B. LUVC exhibits almost no performance degradation, whereas both PACT and VTW show significant declines. Specifically, PACT exhibits a 6.7 PCT decrease in CIDEr score, while VTW shows a 22 PCT reduction with InternVL2.5-8B, indicating diminished content relevance. The observed decrease in BLEU and ROUGE scores corresponds to a substantial deterioration in caption coherence and quality. In contrast, LUVC exhibits only minor reductions of 0.5 and 0.2 in BLEU-1 and BLEU-2 scores, while its CIDEr score surpasses that of PACT by 6.4 percentage points and VTW by 21.7 points. The same experimental conclusion is supported by the results from InternVL2.5-26B. These findings demonstrate that LUVC effectively preserves key semantic information while maintaining a comparable acceleration ratio, thereby sustaining superior model captioning performance—an advantage not achieved by other training-free compression algorithms.

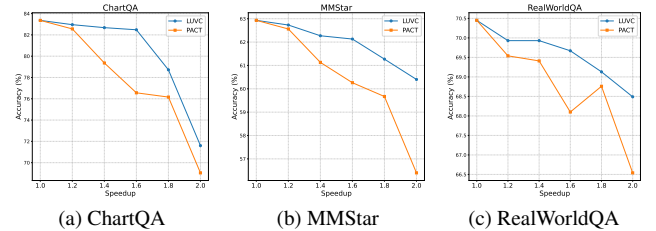


Figure 5. Performance comparison of LUVC and PACT under different **Speedup**.

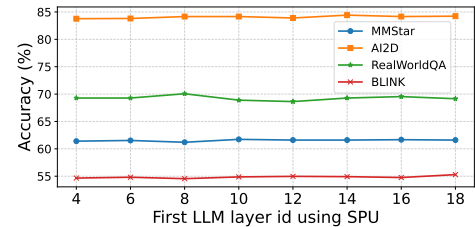


Figure 6. Performance Comparison of LUVC using SPU from different LLM layers.

4.6. Throughput ratio, GPU memory and Algorithm latency

As demonstrated in Table 5, we control comparable performance between PACT/VTW and LUVC by either postponing the initial pruning layer or adjusting pruning thresholds. Under this condition, LUVC attains a Throughput Ratios of 214%, significantly surpassing both PACT and VTW, while simultaneously maintaining the lowest GPU memory.

To provide a more intuitive comparison of the computational latency introduced by different algorithms during model inference, we conducted a comparative analysis of PACT, VTW, and our proposed LUVC. As shown in Table 6, both the algorithm-specific overhead and the over-

Table 5. Throughput Ratios, Red. Ratio, and GPU usage of different methods in InternVL2.5-8B.

Method	No reduction	VTW	PACT	LUVC (ours)
Red. Ratio	0.00%	40.25%	42.00%	56.89%
Throughput Ratio	100%	140%	155%	214%
GPU Memory (GB)	21.79	19.54	19.68	18.68

Table 6. Algorithm and Model Latency (senonds).

Method	VTW	PACT	LUVC	The whole model
InternVL2.5-8B	0.011	0.033	0.031	0.2985
InternVL2.5-26B	0.019	0.062	0.049	0.7454

all model inference latency are presented, with results averaged over multiple test runs using an example image with 12 patches. It can be observed that although LUVC employs an iterative pruning strategy, it does not introduce additional latency burden to the model inference process.

4.7. Ablation Studies

The design of core components of LUVC. First, we compare the performance impact of OIM and SPU using different settings, as shown in Table 7. The experimental results demonstrate that OIM and SPU jointly contribute to the compression efficacy and accuracy maintenance of LUVC. Moreover, value enhancement (VE) and Hamming Window (HW) optimization positively influence OIM and SPU, respectively.

The effect of OIM. Orthogonal Iterative Merging performs orthogonal iterative merging of visual tokens in the spatial scale during ViT. This process can be replaced by 2D downsampling or 2D random selection, and we conduct ablation studies on different strategies as shown in the Table 8. Additionally, we compare the 1D merging strategy of ToMe [3] to achieve a similar compression ratio. As presented in Table 8, ToMe fails to preserve the 2D spatial structure, resulting in disrupted spatial information and severely compromising model performance, with an average metric drop of 2.53 pct. Although 2D downsampling maintains spatial structure, it applies uniform downsampling globally without considering the semantic information of tokens, leading to an average performance decrease of 1.22 pct. We also evaluated a 2D random selection strategy, and the results indicate that random pruning in 2D space cause performance degradation. In contrast, OIM achieves the best performance among all compared methods.

The effect of Speedup. Fig. 5 shows the performance variations of LUVC across ChartQA, RealWorldQA, and MMStar, under different Speedup ratios. As the Speedup increases, the model exhibits a gradual performance decline while maintaining reliable accuracy. For comparison, we also plot the corresponding performance trends of PACT and VTW. The results demonstrate that LUVC consistently

Table 7. Ablation studies on the core components of LUVC.

Method	Latency	Speedup	MMStar	POPE	BLINK	AI2D	Avg.
InternVL-2.5-8B*	0.2985	–	62.93	88.91	54.8	84.5	72.79
+ OIM (wo VE)	0.2615	1.14	60.7	88.46	54.65	83.9	71.93
+ OIM (VE)	0.2615	1.14	61.82	89.11	54.93	84.21	72.52
+ SPU (wo HW)	0.2075	1.44	61.51	89.04	54.66	84.10	72.33
+ SPU (HW)	0.2075	1.44	61.83	89.31	54.65	84.23	72.51
LUVC	0.1658	1.80	61.4	89.19	54.87	84.1	72.39

Table 8. Ablation studies on OIM and other compression methods.

Method	MMStar	POPE	BLINK	AI2D	Avg.
InternVL-2.5-8B*	62.93	88.91	54.8	84.5	72.79
+ ToMe [3]	59.78	84.28	54.00	82.96	70.26
+ 2D random Prune	60.83	87.71	54.07	83.66	71.57
+ nearest interpolate	61.05	88.71	54.24	83.43	71.86
+ bilinear interpolate	61.12	88.31	53.91	83.91	71.81
+ OIM (VE)	61.82	89.11	54.93	84.21	72.52

outperforms these baselines across all Speedup ratios without experiencing abrupt performance degradation.

The effects of initial LLM layer selection for SPU. As illustrated in Fig. 6, we investigate the impact of pruning starting layer selection on model performance based on InternVL2.5-8B during the LLM pruning. Notably, owing to the low computational complexity of FFT, we can implement cascade progressive pruning without causing computational bottlenecks. Experimental results demonstrate that LUVC maintains stable accuracy as the pruning starting layer shifts forward, in stark contrast to algorithms like VTW, which exhibit catastrophic performance collapse when pruning is applied to early-stage layers. This validates the stability and layer-agnostic robustness of LUVC.

5. Conclusion

We propose an ultimate visual tokens compression framework named LUVC based on spectrum theory and spiltal merging. This scheme does not require any training and can be seamlessly integrated into various architectures and parameter quantities of VLMs. LUVC first merges highly similar visual tokens through a orthogonal iterative merge strategy during visual encoding while preserving spatial structural information. Furthermore, LUVC incorporates a dedicated Spectrum Pruning Unit and employs it in a cascaded manner across the LLM. SPU leverages the low-pass filtering property of Transformers to progressively integrate visual information into cross-modal queries by pruning high-frequency redundant tokens. This ultimately achieves complete compression of visual tokens in the LLM. Through its pruning strategy design across all stages, LUVC achieves approximately double the inference speed with minimal accuracy error. Experiments demonstrate that LUVC is applicable to diverse multimodal understanding scenarios, including videos, single images, and multi-images.

References

- [1] Rohan Anil, Sebastian Borgeaud, Yonghui Wu, Jean-Baptiste Alayrac, Jiahui Yu, Radu Soricut, Johan Schalkwyk, Andrew M. Dai, Anja Hauth, Katie Millican, David Silver, Slav Petrov, Melvin Johnson, Ioannis Antonoglou, Julian Schrittwieser, Amelia Glaese, Jilin Chen, Emily Pitler, Timothy P. Lillicrap, Angeliki Lazaridou, Orhan Firat, James Molloy, Michael Isard, Paul Ronald Barham, Tom Hennigan, Benjamin Lee, Fabio Viola, Malcolm Reynolds, Yuanzhong Xu, Ryan Doherty, Eli Collins, Clemens Meyer, Eliza Rutherford, Erica Moreira, Kareem Ayoub, Megha Goel, George Tucker, Enrique Piqueras, Maxim Krikun, Iain Barr, Nikolay Savinov, Ivo Danihelka, Becca Roelofs, Anaïs White, Anders Andreassen, Tamara von Glehn, Lakshman Yagati, Mehran Kazemi, Lucas Gonzalez, Misha Khalman, Jakub Sygnowski, and et al. Gemini: A family of highly capable multimodal models. *CoRR*, 2023. 2
- [2] Shuai Bai, Keqin Chen, Xuejing Liu, Jialin Wang, Wenbin Ge, Sibao Song, Kai Dang, Peng Wang, Shijie Wang, Jun Tang, Humen Zhong, Yuanzhi Zhu, Ming-Hsuan Yang, Zhaohai Li, Jianqiang Wan, Pengfei Wang, Wei Ding, Zheren Fu, Yiheng Xu, Jiabo Ye, Xi Zhang, Tianbao Xie, Zesen Cheng, Hang Zhang, Zhibo Yang, Haiyang Xu, and Junyang Lin. Qwen2.5-vl technical report. *CoRR*, 2025. 1, 2, 4
- [3] Daniel Bolya, Cheng-Yang Fu, Xiaoliang Dai, Peizhao Zhang, Christoph Feichtenhofer, and Judy Hoffman. Token merging: Your vit but faster. In *International Conference on Learning Representations*, 2023. 2, 8
- [4] Lin Chen, Jinsong Li, Xiaoyi Dong, Pan Zhang, Yuhang Zang, Zehui Chen, Haodong Duan, Jiaqi Wang, Yu Qiao, Dahua Lin, and Feng Zhao. Are we on the right way for evaluating large vision-language models? In *Annual Conference on Neural Information Processing Systems*, 2024. 5, 12
- [5] Liang Chen, Haozhe Zhao, Tianyu Liu, Shuai Bai, Junyang Lin, Chang Zhou, and Baobao Chang. An image is worth 1/2 tokens after layer 2: Plug-and-play inference acceleration for large vision-language models. In *European Conference Computer Vision*, 2024. 1, 2, 12
- [6] Zhe Chen, Weiyun Wang, Yue Cao, Yangzhou Liu, Zhangwei Gao, Erfei Cui, Jinguo Zhu, Shenglong Ye, Hao Tian, Zhaoyang Liu, Lixin Gu, Xuehui Wang, Qingyun Li, Yimin Ren, Zixuan Chen, Jiapeng Luo, Jiahao Wang, Tan Jiang, Bo Wang, Conghui He, Botian Shi, Xingcheng Zhang, Han Lv, Yi Wang, Wenqi Shao, Pei Chu, Zhongying Tu, Tong He, Zhiyong Wu, Huipeng Deng, Jiaye Ge, Kai Chen, Min Dou, Lewei Lu, Xizhou Zhu, Tong Lu, Dahua Lin, Yu Qiao, Jifeng Dai, and Wenhui Wang. Expanding performance boundaries of open-source multimodal models with model, data, and test-time scaling. *CoRR*, 2024. 1, 2, 4, 14
- [7] X.AI Corp. Grok-1.5 vision preview: Connecting the digital and physical worlds with our first multimodal model. <https://x.ai/news/grok-1.5v>, 2024. 5, 12
- [8] Tri Dao, Daniel Y. Fu, Stefano Ermon, Atri Rudra, and Christopher Ré. Flashattention: Fast and memory-efficient exact attention with io-awareness. In *Annual Conference on Neural Information Processing Systems*, 2022. 1, 12
- [9] Mohamed Dhoubib, Davide Buscaldi, Sonia Vanier, and Ayman Shabou. PACT: pruning and clustering-based token reduction for faster visual language models. In *Conference on Computer Vision and Pattern Recognition*, 2025. 2, 3, 12
- [10] Chaoyou Fu, Yuhang Dai, Yongdong Luo, Lei Li, Shuhuai Ren, Renrui Zhang, Zihan Wang, Chenyu Zhou, Yunhang Shen, Mengdan Zhang, et al. Video-mme: The first-ever comprehensive evaluation benchmark of multi-modal llms in video analysis. In *Computer Vision and Pattern Recognition*, 2025. 5
- [11] Xingyu Fu, Yushi Hu, Bangzheng Li, Yu Feng, Haoyu Wang, Xudong Lin, Dan Roth, Noah A. Smith, Wei-Chiu Ma, and Ranjay Krishna. BLINK: multimodal large language models can see but not perceive. In *European Conference of Computer Vision*, 2024. 5
- [12] Anwen Hu, Haiyang Xu, Jiabo Ye, Ming Yan, Liang Zhang, Bo Zhang, Ji Zhang, Qin Jin, Fei Huang, and Jingren Zhou. mplug-docowl 1.5: Unified structure learning for ocr-free document understanding. In *Empirical Methods in Natural Language Processing*, 2024. 2
- [13] Peng Jin, Ryuichi Takanobu, Wancai Zhang, Xiaochun Cao, and Li Yuan. Chat-univi: Unified visual representation empowers large language models with image and video understanding. In *Conference on Computer Vision and Pattern Recognition*, 2024. 2, 3
- [14] Aniruddha Kembhavi, Mike Salvato, Eric Kolve, Min Joon Seo, Hannaneh Hajishirzi, and Ali Farhadi. A diagram is worth a dozen images. In *European Conference of Computer Vision*, 2016. 5, 12
- [15] Minchul Kim, Shangqian Gao, Yen-Chang Hsu, Yilin Shen, and Hongxia Jin. Token fusion: Bridging the gap between token pruning and token merging. In *Winter Conference on Applications of Computer Vision*, 2024. 2
- [16] Dan Kondratyuk, Lijun Yu, Xiuye Gu, José Lezama, Jonathan Huang, Grant Schindler, Rachel Hornung, Vignesh Birodkar, Jimmy Yan, Ming-Chang Chiu, Krishna Somandepalli, Hassan Akbari, Yair Alon, Yong Cheng, Joshua V. Dillon, Agrim Gupta, Meera Hahn, Anja Hauth, David Hendon, Alonso Martinez, David Minnen, Mikhail Sirotenko, Kihyuk Sohn, Xuan Yang, Hartwig Adam, Ming-Hsuan Yang, Irfan Essa, Huisheng Wang, David A. Ross, Bryan Seybold, and Lu Jiang. Videopoet: A large language model for zero-shot video generation. In *International Conference on Machine Learning*, 2024. 2
- [17] Bohao Li, Rui Wang, Guangzhi Wang, Yuying Ge, Yixiao Ge, and Ying Shan. Seed-bench: Benchmarking multimodal llms with generative comprehension. *CoRR*, 2023. 5
- [18] Bo Li, Yuanhan Zhang, Dong Guo, Renrui Zhang, Feng Li, Hao Zhang, Kaichen Zhang, Peiyuan Zhang, Yanwei Li, Ziwei Liu, and Chunyuan Li. Llava-onevision: Easy visual task transfer. *Trans. Mach. Learn. Res.*, 2025. 1, 2
- [19] Junnan Li, Dongxu Li, Caiming Xiong, and Steven C. H. Hoi. BLIP: bootstrapping language-image pre-training for unified vision-language understanding and generation. In *International Conference on Machine Learning*, 2022. 2
- [20] Junnan Li, Dongxu Li, Silvio Savarese, and Steven C. H. Hoi. BLIP-2: bootstrapping language-image pre-training

- with frozen image encoders and large language models. In *International Conference on Machine Learning*, 2023. 2
- [21] Kunchang Li, Yali Wang, Yinan He, Yizhuo Li, Yi Wang, Yi Liu, Zun Wang, Jilan Xu, Guo Chen, Ping Luo, et al. Mvbench: A comprehensive multi-modal video understanding benchmark. In *Computer Vision and Pattern Recognition*, 2024. 5
- [22] Yifan Li, Yifan Du, Kun Zhou, Jinpeng Wang, Wayne Xin Zhao, and Ji-Rong Wen. Evaluating object hallucination in large vision-language models. In *Empirical Methods in Natural Language Processing*, 2023. 5, 12
- [23] Bin Lin, Yang Ye, Bin Zhu, Jiaxi Cui, Munan Ning, Peng Jin, and Li Yuan. Video-llava: Learning united visual representation by alignment before projection. In *Empirical Methods in Natural Language Processing*, 2024. 2
- [24] Zhihang Lin, Mingbao Lin, Luxi Lin, and Rongrong Ji. Boosting multimodal large language models with visual tokens withdrawal for rapid inference. In *Annual AAAI Conference on Artificial Intelligence*, 2025. 3, 5, 12
- [25] Haotian Liu, Chunyuan Li, Qingyang Wu, and Yong Jae Lee. Visual instruction tuning. In *Annual Conference on Neural Information Processing Systems*, 2023. 2
- [26] Hao Liu, Wilson Yan, Matei Zaharia, and Pieter Abbeel. World model on million-length video and language with blockwise ringattention. In *International Conference on Learning Representations*, 2025. 2
- [27] Ting Liu, Liangtao Shi, Richang Hong, Yue Hu, Qunjun Yin, and Linfeng Zhang. Multi-stage vision token dropping: Towards efficient multimodal large language model. *CoRR*, 2024. 2
- [28] Yuan Liu, Haodong Duan, Yuanhan Zhang, Bo Li, Songyang Zhang, Wangbo Zhao, Yike Yuan, Jiaqi Wang, Conghui He, Ziwei Liu, Kai Chen, and Dahua Lin. Mmbench: Is your multi-modal model an all-around player? In *European Conference of Computer Vision*, 2024. 5
- [29] Ahmed Masry, Do Xuan Long, Jia Qing Tan, Shafiq Joty, and Enamul Hoque. Chartqa: A benchmark for question answering about charts with visual and logical reasoning. In *Annual Meeting of the Association for Computational Linguistics*, 2022. 5, 12
- [30] Minesh Mathew, Dimosthenis Karatzas, and CV Jawahar. Docvqa: A dataset for vqa on document images. In *Winter conference on Applications of Computer Vision*, pages 2200–2209, 2021. 5, 12
- [31] Minesh Mathew, Viraj Bagal, Rubèn Tito, Dimosthenis Karatzas, Ernest Valveny, and CV Jawahar. Infographicvqa. In *Winter conference on Applications of Computer Vision*, 2022. 5
- [32] OpenAI. GPT-4 technical report. *CoRR*, abs/2303.08774, 2023. 1
- [33] Alec Radford, Jong Wook Kim, Chris Hallacy, Aditya Ramesh, Gabriel Goh, Sandhini Agarwal, Girish Sastry, Amanda Askell, Pamela Mishkin, Jack Clark, Gretchen Krueger, and Ilya Sutskever. Learning transferable visual models from natural language supervision. In *International Conference on Machine Learning*, 2021. 1
- [34] Yongming Rao, Wenliang Zhao, Benlin Liu, Jiwen Lu, Jie Zhou, and Cho-Jui Hsieh. Dynamicvit: Efficient vision transformers with dynamic token sparsification. In *Annual Conference on Neural Information Processing Systems*, 2021. 2
- [35] Yuzhang Shang, Mu Cai, Bingxin Xu, Yong Jae Lee, and Yan Yan. Llava-prumerge: Adaptive token reduction for efficient large multimodal models. *CoRR*, 2024. 3
- [36] Amanpreet Singh, Vivek Natarajan, Meet Shah, Yu Jiang, Xinlei Chen, Dhruv Batra, Devi Parikh, and Marcus Rohrbach. Towards vqa models that can read. In *Computer Vision and Pattern Recognition*, 2019. 5
- [37] Chau Tran, Duy M. H. Nguyen, Manh-Duy Nguyen, TrungTin Nguyen, Ngan Le, Pengtao Xie, Daniel Sonntag, James Y. Zou, Binh Nguyen, and Mathias Niepert. Accelerating transformers with spectrum-preserving token merging. In *Annual Conference on Neural Information Processing Systems*, 2024. 2
- [38] Pavan Kumar Anasosalu Vasu, Fartash Faghri, Chun-Liang Li, Cem Koc, Nate True, Albert Antony, Gokula Santhanam, James Gabriel, Peter Grasch, Oncel Tuzel, and Hadi Pouransari. Fastvlm: Efficient vision encoding for vision language models. In *Computer Vision and Pattern Recognition*, 2025. 3
- [39] Fei Wang, Xingyu Fu, James Y. Huang, Zekun Li, Qin Liu, Xiaogeng Liu, Mingyu Derek Ma, Nan Xu, Wenxuan Zhou, Kai Zhang, Tianyi Lorena Yan, Wenjie Jacky Mo, Hsiang-Hui Liu, Pan Lu, Chunyuan Li, Chaowei Xiao, Kai-Wei Chang, Dan Roth, Sheng Zhang, Hoifung Poon, and Muhao Chen. Muirbench: A comprehensive benchmark for robust multi-image understanding. In *International Conference on Learning Representations*, 2025. 5
- [40] Peihao Wang, Wenqing Zheng, Tianlong Chen, and Zhangyang Wang. Anti-oversmoothing in deep vision transformers via the fourier domain analysis: From theory to practice. In *International Conference on Learning Representations*, 2022. 2, 4
- [41] Peng Wang, Shuai Bai, Sinan Tan, Shijie Wang, Zhihao Fan, Jinze Bai, Keqin Chen, Xuejing Liu, Jialin Wang, Wenbin Ge, Yang Fan, Kai Dang, Mengfei Du, Xuancheng Ren, Rui Men, Dayiheng Liu, Chang Zhou, Jingren Zhou, and Junyang Lin. Qwen2-vl: Enhancing vision-language model’s perception of the world at any resolution. *CoRR*, 2024. 3, 12
- [42] Yi Wang, Xinhao Li, Ziang Yan, Yinan He, Jiashuo Yu, Xiangyu Zeng, Chenting Wang, Changlian Ma, Haian Huang, Jianfei Gao, Min Dou, Kai Chen, Wenhai Wang, Yu Qiao, Yali Wang, and Limin Wang. Internvideo2.5: Empowering video mllms with long and rich context modeling. *CoRR*, 2025. 2
- [43] Zichen Wen, Yifeng Gao, Weijia Li, Conghui He, and Linfeng Zhang. Token pruning in multimodal large language models: Are we solving the right problem? In *Association for Computational Linguistics*, 2025. 1, 4
- [44] Haoning Wu, Dongxu Li, Bei Chen, and Junnan Li. Longvideobench: A benchmark for long-context interleaved video-language understanding. In *Annual Conference on Neural Information Processing Systems*, 2024. 5
- [45] Junbin Xiao, Xindi Shang, Angela Yao, and Tat-Seng Chua. Next-qa: Next phase of question-answering to explaining

- temporal actions. In *Computer Vision and Pattern Recognition*, 2021. 5
- [46] Yifan Xu, Zhijie Zhang, Mengdan Zhang, Kekai Sheng, Ke Li, Weiming Dong, Liqing Zhang, Changsheng Xu, and Xing Sun. Evo-vit: Slow-fast token evolution for dynamic vision transformer. In *Annual AAAI Conference on Artificial Intelligence*, 2022. 2
- [47] Senqiao Yang, Yukang Chen, Zhuotao Tian, Chengyao Wang, Jingyao Li, Bei Yu, and Jiaya Jia. Visionzip: Longer is better but not necessary in vision language models. In *Conference on Computer Vision and Pattern Recognition*, 2025. 2
- [48] Yuan Yao, Tianyu Yu, Ao Zhang, Chongyi Wang, Junbo Cui, Hongji Zhu, Tianchi Cai, Haoyu Li, Weilin Zhao, Zhihui He, Qianyu Chen, Huarong Zhou, Zhensheng Zou, Haoye Zhang, Shengding Hu, Zhi Zheng, Jie Zhou, Jie Cai, Xu Han, Guoyang Zeng, Dahai Li, Zhiyuan Liu, and Maosong Sun. Minicpm-v: A GPT-4V level MLLM on your phone. *CoRR*, 2024. 2, 3
- [49] Dong Yin, Raphael Gontijo Lopes, Jonathon Shlens, Ekin Dogus Cubuk, and Justin Gilmer. A fourier perspective on model robustness in computer vision. In *Annual Conference on Neural Information Processing Systems*, 2019. 4
- [50] Peter Young, Alice Lai, Micah Hodosh, and Julia Hockenmaier. From image descriptions to visual denotations: New similarity metrics for semantic inference over event descriptions. *Trans. Assoc. Comput. Linguistics*, 2014. 5, 7
- [51] Xiang Yue, Yuansheng Ni, Tianyu Zheng, Kai Zhang, Ruochi Liu, Ge Zhang, Samuel Stevens, Dongfu Jiang, Weiming Ren, Yuxuan Sun, Cong Wei, Botao Yu, Ruibin Yuan, Renliang Sun, Ming Yin, Boyuan Zheng, Zhenzhu Yang, Yibo Liu, Wenhao Huang, Huan Sun, Yu Su, and Wenhua Chen. MMMU: A massive multi-discipline multimodal understanding and reasoning benchmark for expert AGI. In *Computer Vision and Pattern Recognition*, 2024. 5
- [52] Xiaohua Zhai, Basil Mustafa, Alexander Kolesnikov, and Lucas Beyer. Sigmoid loss for language image pre-training. In *International Conference on Computer Vision*, 2023. 1
- [53] Liang Zhang, Anwen Hu, Haiyang Xu, Ming Yan, Yichen Xu, Qin Jin, Ji Zhang, and Fei Huang. Tinychart: Efficient chart understanding with program-of-thoughts learning and visual token merging. In *Empirical Methods in Natural Language Processing*, 2024. 2
- [54] Liang Zhang, Anwen Hu, Haiyang Xu, Ming Yan, Yichen Xu, Qin Jin, Ji Zhang, and Fei Huang. Tinychart: Efficient chart understanding with program-of-thoughts learning and visual token merging. In *Empirical Methods in Natural Language Processing*, 2024. 2
- [55] Qizhe Zhang, Aosong Cheng, Ming Lu, Zhiyong Zhuo, Minqi Wang, Jiajun Cao, Shaobo Guo, Qi She, and Shanghang Zhang. [cls] attention is all you need for training-free visual token pruning: Make vlm inference faster. *arXiv preprint arXiv:2412.01818*, 2024. 1, 3
- [56] Yuan Zhang, Chun-Kai Fan, Junpeng Ma, Wenzhao Zheng, Tao Huang, Kuan Cheng, Denis Gudovskiy, Tomoyuki Okuno, Yohei Nakata, Kurt Keutzer, et al. Sparsevlm: Visual token sparsification for efficient vision-language model inference. In *International Conference on Machine Learning*, 2025. 1, 3
- [57] Dehua Zheng, Wenhui Dong, Hailin Hu, Xinghao Chen, and Yunhe Wang. Less is more: Focus attention for efficient DETR. In *International Conference on Computer Vision*, 2023. 2
- [58] Junjie Zhou, Yan Shu, Bo Zhao, Boya Wu, Shitao Xiao, Xi Yang, Yongping Xiong, Bo Zhang, Tiejun Huang, and Zheng Liu. MLVU: A comprehensive benchmark for multi-task long video understanding. *CoRR*, 2024. 5

6. Appendix

6.1. Experiments on Qwen2-VL-7B-Instruct

To further validate the generalizability of our proposed LUVc across diverse VLM architectures, we conduct additional experiments on Qwen2-VL-7B-Instruct [41]. As shown in the Table 9, we evaluate six datasets, including MMStar [4], AI2D [14], RealWorldQA [7], DocVQA [30], POPE [22], and ChartQA [29], spanning single-image, multi-image, and dense document understanding tasks. The latency is measured on 100 randomly sampled documents from DocVQA, with mean processing times computed for each algorithm on GPU. The experimental results demonstrate that, under comparable speedup ratios, LUVc achieves an average performance improvement of **+2.52** over PACT, the state-of-the-art similarity-aware method, while surpassing the attention-aware representative method FastV by **+3.32**. Additionally, it outperforms VTW by **+24.45** percentage points, respectively. To date, LUVc has undergone extensive experimental validation across VLM models from the Qwen2VL, InternVL2.5, and LLaVA-OV series. Substantial evidence confirms that the proposed SPU and OIM strategies in LUVc deliver robust and stable performance in accelerating VLM inference.

6.2. Implementation Details of Other Methods

For PACT [9]. As described in the PACT, the authors conducted validation experiments on the Qwen2-VL-7B, InternVL2-8B, and LLaVA-OV-7B. We reused their original settings and reproduced the publicly reported performance using the open-source code on LLaVA-OV-7B and Qwen2-VL-7B. Given the architectural consistency between InternVL2 and InternVL2.5, we applied the same parameter configurations from InternVL2-8B to InternVL2.5-8B, achieving comparable performance (including publicly reported metrics such as speedup and performance degradation). For LLaVA-OV-0.5B, since the authors did not provide relevant experiments, we adjusted the pruning starting layer. Using the settings from LLaVA-OV-7B led to performance collapse, so we select the 8th layer to achieve stable performance. Similarly, for InternVL2.5-26B, we chose the 11th layer as the starting pruning layer to ensure stable performance.

For FastV [5]. The core principle of the FastV lies in its text-guided visual pruning mechanism based on text-image attention. The authors operate pruning at the second layer of the LLM. However, given that modern computational architectures have moved away from traditional attention computation in favor of optimized approaches such as FlashAttention [8], we adapt the method for LLaVA-OV and Qwen2VL series by retaining the relevant query and key matrices to recompute the attention required by FastV. To achieve an optimal balance between pruning depth and

model performance, we systematically adjusted the selection of pruned layers. Specifically, for LLaVA-OV-0.5B, we retain the original design proposed by the authors, implementing pruning at the second layer. In contrast, for both LLaVA-OV-7B and Qwen2-VL-7B, we strategically shift the pruning layer to the fourth layer to enhance performance stability. This deliberate layer selection strategy ensures robust performance preservation while maintaining computational efficiency under the constraints of contemporary attention mechanisms.

For VTW [24]. The VTW algorithm posits that visual tokens become increasingly redundant in later layers of LLMs. The researchers employed a meticulously designed pruning layer selection strategy to identify the optimal starting layer for discarding all visual tokens. In our reproduction of their method, we fine-tuned the pruning layer within a window around the originally suggested position to achieve the best balance between performance and inference speed. Specifically, we identified the following optimal pruning layers for each model:

- LLaVA-OV-0.5B: Layer 8
- LLaVA-OV-7B/Qwen2-VL-8B: Layer 12
- InternVL2.5-8B: Layer 14
- InternVL2.5-26B: Layer 20

This configuration is carefully designed to minimize adverse effects on model performance while preventing potential performance collapse. The layer selection follows a clear scaling pattern correlated with model size, demonstrating that larger-scale models preserve their representational capacity by implementing pruning at later stages.

6.3. Evaluation Datasets and Metrics

We conduct extensive evaluations across multiple benchmarks. We summarize their respective evaluation metrics, as detailed in the Table 10. The ANLS (Average Normalized Levenshtein Similarity) metric serves as the standard evaluation criterion in DocVQA and InfoVQA tasks, quantifying the similarity between model-generated answers and reference answers. It is noteworthy that, to ensure a fair and objective comparison of algorithm performance, we have excluded benchmarks that require third-party model evaluation.

6.4. Iterative Strategy and Pseudocode of OIM

As shown in the Algorithm 1, we demonstrate the detailed process of orthogonal iterative merging (OIM) execution. For the visual encoder, we opt to merge visually similar tokens at the intermediate stage of the network. We employ an alternating iterative strategy for merging the height and width dimensions, with the merge number configured as 2. In each OIM in spatial axes, one height-dimension merging and one width-dimension merging are performed. The number of OIM operations is set to 3 for video scenes, while for

Method	Latency	Speedup	MMStar	AI2D	RealWorldQA	DocVQA	ChartQA	POPE	Avg.
Qwen2VL-7B-Instruct	0.3569	–	56	79.9	65.1	93.9	80.8	88.58	77.38
+FastV	0.3594	0.99×	51.5	76.2	63.81	86.6	75.32	85.76	73.20
+VTW	0.2437	1.46×	55.7	77.4	64.18	10.84	18.12	86.19	52.07
+PACT	0.2179	1.64×	54.8	78.4	58.95	90.5	76	85.35	74
+ LUVc (ours)	0.2335	1.53×	55.66	78.86	65.23	91.33	80.08	87.98	76.52

Table 9. Comparative of LUVc with FastV, VTW, and PACT on Qwen2VL-7B. **Latency** represents the prefill latency of the LLM, and **Speedup** indicates the acceleration ratio. Herein, the best performance is highlighted in **bold**.

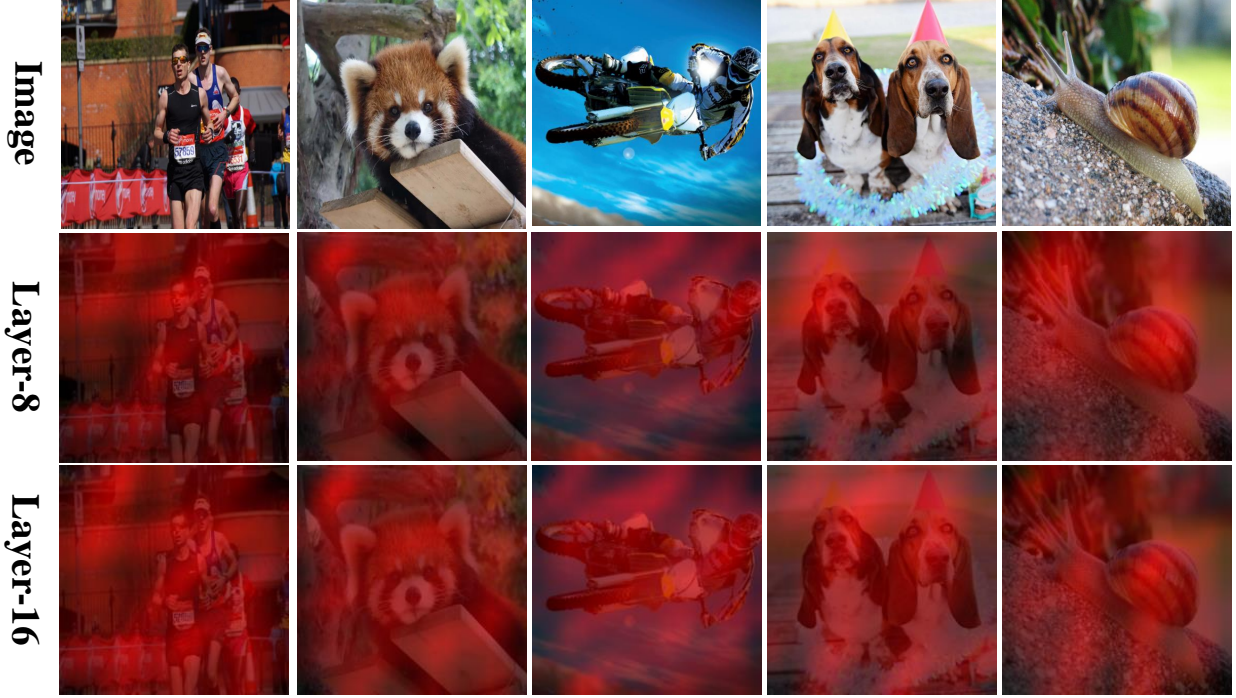


Figure 7. The visualization results of the mapping relationship between low-frequency visual tokens and the original image. These results were obtained from different LLM layers of InternVL2.5-8B.

Benchmark	Split	Metric
VideoMME	–	Acc.
MVBench	–	Acc.
NextQA	MC	Acc.
SeedBench	Video	Acc.
MLVU	–	Acc.
LongVideo	–	Acc.
MMB	Val	Acc.
POPE	–	F1
MMStar	–	Acc.
MMMUNVal	Val	Acc.
AI2D	–	Acc.
MuirBench	–	Acc.
BLINK	–	Acc.
RealWorld	–	Acc.
ChartQA	Val	Relaxed Acc.
DocVQA	Val	ANLS
InfoVQA	Val	ANLS
TextVQA	Val	Official metric

Table 10. Dataset Splits, and Evaluation Metrics Used in Our Experiments.

text-image scenes, it can be adjusted to either 1 or 2. We have established a flexible parameter adjustment strategy that can be controlled according to different acceleration requirements.

Specifically, for the Qwen2VL model, due to its adoption of the anyres strategy, we no longer employ a fixed number of merges. Instead, the merging operations along the spatial dimensions are dynamically adjusted based on the aspect ratio of the input image.

6.5. Pseudocode of Low-Frequency Filter in SPU

As illustrated in the Algorithm 2, we provide a detailed demonstration of the spectrum pruning unit (SPU) execution process. For SPU operations, we configure two key parameters: the initial pruning layer (l_0) and the pruning interval (l_δ). Specifically:

- LLaVA-0.7/7B and Qwen2VL-7B: $l_0=8$; $l_\delta=3$
- InternVL2.5-8B: $l_0=6$; $l_\delta=3$

Algorithm 1 Orthogonal Iterative Merging

Input: $T_v \in R^{n_v \times D}$

Parameter: r , the number to merge in each spatial axes
 l_i , the layer index of visual encoder
 L_h , the visual encoder layers to operate merging in height.
 L_w , the visual encoder layers to operate merging in width.

```
1: for i,j in zip( $L_h, L_w$ ) do  
2:   assert j=i+1  
3: end for
```

Output: The visual tokens T'_v after Orthogonal Iterative Merging.

Define:

MLP_{qkv} : The map function of qkv.

FA : Flash Attention

s : vector containing the number of the merged tokens.

OIM_h : Orthogonal Iterative Merging in height.

OIM_w : Orthogonal Iterative Merging in width.

```
2: if  $l_i$  in  $L_h$  then  
    $q, k, v = MLP_{qkv}(T_v)$   
4:    $T'_v = FA(q, k, v + \log(s))$   
    $T'_v = OIM_h(T'_v)$   
6: else if  $l_i$  in  $L_w$  then  
    $q, k, v = MLP_{qkv}(T_v)$   
8:    $T'_v = FA(q, k, v + \log(s))$   
    $T'_v = OIM_w(T'_v)$   
10: else  
   continue.  
12: end if
```

• InternVL2.5-26B: $l_0=14$; $l_\delta=4$

6.6. More Visualisation of Low-Frequency Vision Tokens

As illustrated in Fig. 7, we test additional images and analyzed the visualization results of low-frequency visual tokens mapped back to the original images across different LLM layers of InternVL2.5-8B [6]. Here, we employed the same prompt: "Please describe the image shortly." The visualization results clearly demonstrate that low-frequency visual tokens encode richer visual semantics and retain more critical information, further supporting the reliability of the SPU strategy adopted in LUVc.

Algorithm 2 Spectrum Pruning Unit

Input: $T_v \in R^{n_v \times D}$

Parameter: n'_v , the visual token length to keep

l_i , the layer index of LLM

L_p , the all LLM layers to operate low-pass filtering

Output: Low-frequency visual tokens T'_v .

1: Define:

FFT: Fast Fourier Transform;

IFFT: Inverse Fast Fourier Transform.

HW: Hamming Window.

2: **if** l_i in L_p **then**

3: $F_v = FFT(T_v)$, get frequency-domain feature of T_v

4: $F'_v = HW(F_v)$, get low-frequency feature F'_v .

5: $T'_v = IFFT(F'_v)$, get low-frequency tokens T'_v .

6: $E_v = ||(T'_v)||_2$, get the energy E_v of visual tokens.

7: $IDX_l = \text{topk}(E_v, n'_v).index$

8: $T'_v = T_v[IDX_l]$

9: **else**

10: **continue.**

11: **end if**
